Published in final edited form as:

Mater Sci Eng C Mater Biol Appl. 2013 December 1; 33(8): 4767–4776. doi:10.1016/j.msec.2013.07.037.

Characterization of thermoplastic polyurethane/polylactic acid (TPU/PLA) tissue engineering scaffolds fabricated by microcellular injection molding

Hao-Yang Mi[a,b], **Max R. Salick**[c], **Xin Jing**[a,b], **Brianna R. Jacques**[d], **Wendy C. Crone**[c], **Xiang-Fang Peng**[a,*], and **Lih-Sheng Turng**[b,*]

[a]National Engineering Research Center of Novel Equipment for Polymer Processing, South China University of Technology, Guangzhou, China

[b]Department of Mechanical Engineering, University of Wisconsin–Madison, WI, USA

[c]Department of Engineering Physics, University of Wisconsin–Madison, WI, USA

[d]Department of Biology, University of Wisconsin–River Falls, WI, USA

Abstract

Polylactic acid (PLA) and thermoplastic polyurethane (TPU) are two kinds of biocompatible and biodegradable polymers that can be used in biomedical applications. PLA has rigid mechanical properties while TPU possesses flexible mechanical properties. Blended TPU/PLA tissue engineering scaffolds at different ratios for tunable properties were fabricated via twin screw extrusion and microcellular injection molding techniques for the first time. Multiple test methods were used to characterize these materials. Fourier transform infrared spectroscopy (FTIR) confirmed the existence of the two components in the blends; differential scanning calorimetry (DSC) and dynamic mechanical analysis (DMA) confirmed the immiscibility between the TPU and PLA. Scanning electron microscopy (SEM) images verified that, at the composition ratios studied, PLA was dispersed as spheres or islands inside the TPU matrix and that this phase morphology further influenced the scaffold's microstructure and surface roughness. The blends exhibited a large range of mechanical properties that covered several human tissue requirements. 3T3 fibroblast cell culture showed that the scaffolds supported cell proliferation and migration properly. Most importantly, this study demonstrated the feasibility of mass producing biocompatible PLA/TPU scaffolds with tunable microstructures, surface roughnesses, and mechanical properties that have the potential to be used as artificial scaffolds in multiple tissue engineering applications.

Keywords

Polylactic acid (PLA); Thermoplastic polyurethane (TPU); Microcellular injection molding; Tissue engineering scaffold; Fibroblasts

*Corresponding authors. Tel.: +1 608 316 4310. pmxfpeng@scut.edu.cn (X.-F. Peng), turng@engr.wisc.edu (L.-S. Turng).

1. Introduction

Tissue engineering aimed at the regeneration of malfunctioning tissues is attracting more and more attention [1,2]. So far, tissue engineering has already been used to improve the recovery of different types of tissues such as skin, bones, blood vessels, and nerve conduits [3]. Currently, the main challenge for tissue engineered scaffolds is the need to mass produce three-dimensional (3D) highly porous scaffolds with suitable surface properties that promote the biological activities of both seeded and native cells. These biological activities, such as cell adhesion, proliferation, migration, and differentiation, are greatly affected by the surrounding extracellular matrices (ECM), and these responses must be tuned to fulfill the requirements of the targeted tissue [4]. The optimal pore size for tissue regeneration depends on the type of tissue [5]. However, the porosity and mechanical properties, which are both important traits of tissue engineering scaffolds, are closely interrelated. The mechanical properties need to closely match those of the real tissue in order to provide support during the initial stages of tissue growth. The mechanical properties of several tissues are listed in Table 1, indicating a large mechanical property range among a variety of human tissues [5-7]. Surface chemistry properties are also crucial for tissue engineering scaffolds. It has been reported that improvement of surface hydrophilicity, roughness, and chemistry by methods such as surface grafting, surface modification, physical blending, and surface crystallization, can help to improve cell adhesion as well as biocompatibility [8-11].

Commonly used biocompatible and biodegradable materials can be classified into natural materials including proteins like collagen [12], polysaccharides like chitosan [13], and synthesized polymers such as polylactide acid (PLA) [14], polycaprolactone (PCL) [15], polyglycolide (PLG) [16], polylactic-co-glycolic acid (PLGA) [17], and polyurethane (PU) [18]. PLA been widely used in the tissue engineering scaffold field in order to promote bone regeneration [19], and to provide scaffolding for blood vessels [20] and cartilage [21]. However, PLA alone usually can only be used in hard tissue engineering scaffolds due to its inherent high strength and brittle properties. Researchers have been focusing on fabricating polymer blends such as PLA/PCL [22], PLA/collagen [23], PLA/chitosan [24], and PLA/PLGA [25], and polymer composites like PLA/hydroxyapatite (HA) [26] and PLA/carbon nanotubes (CNT) [27] scaffolds with adjustable microstructures, physical properties, and chemical properties to match specific tissue applications. Bioresorbable PU scaffolds have attracted considerable attention and their great potential in tissue engineering has been reported [28,29]. Thermoplastic polyurethane (TPU) as a class of PU has been widely employed in medical applications due to its biocompatibility and flexibility, and has been used in medical devices such as catheters [30], pace-maker leads [31], skin [32], and vascular grafts [33]. TPUs offer high elongation, moderate tensile strength and Young's modulus, and excellent abrasion and tear resistance [34]. Thus the combination of PLA and TPU in various ratios would lead to tailored properties suitable for a wide variety of tissue engineering scaffold applications (e.g., for healing and regeneration of cartilage and bones). The biocompatibility and tissue response of PLA-based polyurethane have been studied [35], while blends of PLA and TPU used as tissue engineering scaffolds are still poorly understood. It has been reported that the properties of PLA would change dramatically after the addition of TPU [36].

Several methods have been used in tissue engineering scaffold fabrication, including solvent casting/particulate leaching [37], thermally induced phase separation [38], electrospinning [39], rapid prototyping [40], batch foaming [41], and microcellular injection molding [6,42]. TPU scaffolds fabricated via microcellular injection molding have been studied recently [43]. In this study, PLA/TPU scaffolds with various properties were mass produced with microcellular injection molding for the first time to explore their suitability for various tissue engineering applications. The miscibility, tunable mechanical properties, and biocompatibility were investigated.

2. Materials and methods

2.1. Materials

TPU (Elastollan 1185A, BASF Ltd., USA) is a flexible elastomer that provides flexibility to the blends. Its glass transition temperature (T_g) is −50 °C (based on DSC test), weight average molecular weight (M_w) is 108.5 kDa, and polydispersity index (PDI) is 2.26 (based on GPC test). PLA (3001D, NatureWorks LLC., USA) was selected to improve the rigidity of the blends. Its T_g is 60 °C (based on DSC test), M_w is 127.1 kDa, and PDI is 1.6 (based on GPC test). Both TPU and PLA have similar melt processing windows, allowing them to be compounded properly.

2.2. Scaffold fabrication

2.2.1. Compounding—The TPU and PLA pellets were dried at 100 °C with circular air flow for 2 h prior to compounding. Materials with a variety of formulas – PLA, PLA75% (75%PLA/25%TPU), PLA50% (50%PLA/50%TPU), PLA25% (25%PLA/75%TPU), and TPU – were compounded with a twin-screw extruder (Leistritz ZSE 18 HPe) at 190 °C (the die temperature) at a screw speed of 100 rad/min, followed by circular water cooling and granulation.

2.2.2. Microcellular injection molding—The injection molding machine used was an Arburg Allrounder 320S with a 25 mm diameter screw and a mold temperature controlling device. The machine was equipped with a supercritical carbon dioxide (CO_2) supply system (MuCell® Trexel, Inc.) which enabled precise control of the gas injection weight by adjusting the gas flow rate and valve open time. The mold used in this experiment had a standard ASTM D638 Type I tensile test bar cavity and an ASTM D790 flexural test bar cavity. The pre-blended pellets were dried for 3 h at 100 °C to remove the moisture before being used for microcellular injection molding. Both solid and foamed samples were collected. The processing parameters for the microcellular injection molding procedure are listed in Table 2.

2.3. NIH 3T3 fibroblast cell culture

PLA, PLA50%, and TPU scaffolds were chosen for cell culture testing in order to investigate the biocompatibility and cell viability on pure materials and on PLA/TPU blends. NIH 3T3 ECACC cells were maintained prior to testing on 6-well tissue culture-treated polystyrene plates (BD Falcon). Cells were fed every other day with a high-glucose 20% serum medium consisting of high-glucose DMEM (Gibco), 20% fetal bovine serum

(WiCell), 2 mM L-glutamine (Invitrogen), and penicillin–streptomycin (Invitrogen). Cells were passaged at a 1:40 ratio every 6 days via 5-minute EDTA treatment (Invitrogen). Maintained cultures were regularly checked for mycoplasma. Test samples were placed in 24-well tissue culture-treated polystyrene plates after autoclave sterilization considering that UV light may not be able to penetrate and sterilize the inner part of the 3D scaffold. 3T3 cells were treated with EDTA for 5 min and washed with phosphate-buffered saline (PBS) prior to seeding. Cells were then seeded at a density of 1.25×10^5 cells/cm^2 in the high-glucose 3T3 medium described above. Spent medium was aspirated and replaced with 1 mL of fresh medium daily for screening samples.

2.4. Characterizations

2.4.1. Fourier transform infrared spectroscopy (FTIR)—FTIR measurements were carried out using a Bruker Tensor 27 instrument. The samples were analyzed in absorbance mode in the range of 600 to 4000 cm^{-1}. The functionalities corresponding to each of the absorption bands were analyzed.

2.4.2. Differential scanning calorimetry (DSC)—Thermal property measurements were performed with a DSC Q20 (TA Instruments). Samples were placed in standard aluminum pans and covered with lids. Samples were then heated to 220 °C at a heating rate of 10 °C/min and held isothermally for 5 min to remove any prior thermal history. Samples were then cooled to −80 °C at 5 °C/min and heated to 220 °C at 10 °C/min. All tests were carried out under the protection of a nitrogen atmosphere.

2.4.3. Dynamic mechanical analysis (DMA)—Thermal dynamic properties of the samples were examined in single cantilever mode by a TA Instrument DMAQ 800. The samples were trimmed to 35.6 mm long by 12.8 mm wide by 3.2 mm thick. The tests were performed at a temperature range from −60 °C to 150 °C at a heating rate of 5 °C/min with a frequency of 1 Hz. Liquid nitrogen was used to regulate temperature during heating and cooling.

2.4.4. Scanning electron microscopy (SEM)—The phase morphology of solid samples and the microstructure of microcellular injection molded samples were evaluated using a JEOL Neoscope SEM (Nikon) with an accelerating voltage of 10 kV. All specimens were frozen in liquid nitrogen and broken by two clamps to expose the cross section at the center of the flexural test parts. SEM observations were performed after sputtering the samples with a thin film of gold for 40 s.

The morphology indices of the microcellular injection molded samples (scaffolds) were measured from SEM pictures using the Image Proplus software package. Pores generated in the microcellular injection molding process are typically referred to as ‘cells,’ but will be referred to as ‘pores’ in this paper to avoid confusion with biological cells. Thus, the pore diameter and pore density were used to describe the morphological properties of the scaffolds.

Eq. (1) was used to convert surface average diameter to volume average diameter.

$$D^3=\frac{1}{n}\sum_{i=1}^{n}D_i^3 \quad (1)$$

Eq. (2) was used to calculate volumetric pore density,

$$\text{Pore density}=\left(\frac{N}{A}\right)^{\frac{3}{2}} \quad (2)$$

where N was the number of pores and *A* was the area of the SEM image.

2.4.5. Porosity measurement—Microcellular injection molded samples were trimmed into rectangles and their porosity was determined by weighing the samples and measuring their dimensions to obtain their volume using Eq. (3). The porosity was the mean value of five samples,

$$\text{Porosity}=\frac{V_{th}\rho-W_m}{V_{th}\rho}\times 100\% \quad (3)$$

where W_m was the measured weight, ρ was the weight average density of the blends, and V_{th} was the volume of the microcellular injection molded sample.

2.4.6. Mechanical properties—Tensile tests of ASTM tensile test bars were performed on a mechanical testing machine (Instron 5967) under dry conditions according to the standard test method for tensile properties (ASTM D638) of plastics. The tests were performed at ambient temperature (23 °C) with a cross-head speed of 50 mm/min. A maximum 600% tensile strain was set as the termination criterion of the test due to instrument limitations. The same instrument was outfitted with compressive clamps for compression tests of rectangular samples following the standard test method (ASTM D695). All samples were compressed to 50% strain at a speed of 5 mm/min. Statistical results were the average of the five samples.

2.4.7. Gel permeation chromatography (GPC)—A model VE2001 gel permeation chromatographer (GPC) with model 302 tetra detector array was used to test the molecular weight of the TPU and PLA samples before processing, after microcellular injection molding, and after autoclaving, in order to investigate the potential degradation of the materials from each of the procedures. Tetrahydrofuran (THF) was used as a mobile phase at a flow rate of 1.0 mL/min. Calibrations of columns were carried out using a standard polystyrene (PS) solution. All test solutions were prepared at a concentration of 1.5% (g/ml).

2.4.8. Rheology test—The viscosity of the pure material and the blends were tested via a rheometer (AR 2000ex). A 25 mm parallel-plate geometry was used and all of the tests were performed at 190 °C. The complex viscosity was investigated with the increase of angular frequency from 0.1 to 200 rad/s.

2.4.9. 3T3 fibroblast cell viability—Fibroblast cell viability was determined 3 days and 10 days after seeding. Viability was assessed via a Live/Dead Viability/Cytotoxicity Kit

(Invitrogen). The stain utilized green fluorescent Calcein-AM to target esterase activity within the cytoplasm of living cells, and red fluorescent ethidium homodimer-1 (EthD-1) to indicate cell death by penetrating damaged cell membranes. Stained cells were imaged with a Nikon Eclipse Ti Microscope with an attached Photometrics CoolSNAP HQ2 camera. Nis-D Elements Advanced Research v.3.22 software was used for image analysis.

2.4.10. Cell fixation for SEM—The same samples used for cell viability testing were rinsed twice with Hanks' balanced salt solution (HBSS; Thermo Scientific). HyClone HyPure molecular biology grade water (Thermo Scientific) was mixed with paraformaldehyde to make a 4% solution. The rinsed samples were then immersed in the solution for 30 min. The samples were dehydrated using a series of ethanol washes (50%, 80%, 90%, and 100% for 30 min each), and finally dried in a vacuum desiccator for 2 to 3 h before gold sputtering for SEM.

2.4.11. MTS assay—CellTiter 96 Aqueous One Solution Cell Proliferation Assay (Promega) was used to determine the number of cells during culture on the novel materials. This assay utilizes a tetrazolium compound that is bioreduced upon entering a cell. The resulting products predictably alter the absorbance of the media in which the cells reside. Standard curves were established by performing the tests on cells seeded on the cell culture wells without scaffolds and confirmed by comparison to hemocytometer readings prior to these experiments. Upon testing, cells were treated with an 83% media, 17% MTS solution and allowed to incubate for exactly one hour. After incubation, 100 μL of spent media were removed and added to a clear 96-well plate. The absorbance of this plate at the 450 nm wavelength was then read with a GloMax-Multi + Multiplate Reader (Promega) and the subsequent number of cells was determined relative to the negative control. Positive control was not necessary according to the protocol. The Student's-*t* test ($p < 0.05$) was used to determine the cell number and its statistical significance between samples at the same time interval.

3. Results and discussion

3.1. Immiscibility of TPU and PLA

3.1.1. FTIR result—FTIR was used to identify the molecular construction of the blends. As shown in Fig. 1, the peak at 3332 cm^{-1}, which indicates the N–H group in urethane (–NHCOO–), and the peaks at 2935 and 2850 cm^{-1}, which belong to the asymmetric and symmetric vibration of the –CH2 group, respectively, are the characteristic peaks of TPU. Their intensity increases with increasing TPU ratio [44]. The –C=O group peak at 1748 cm^{-1} only exists in PLA and its intensity decreases with increasing TPU ratio [45]. The FTIR results showed that PLA and TPU were compounded successfully and that no chemical reactions occurred during melt blending since no new chemical bonds were identified.

The miscibility and phase morphology of the polymer blends are very important factors and could influence the properties of the blends. Three methods including DSC, DMA, and SEM were used to study the miscibility and phase morphology of PLA and TPU.

3.1.2. DSC and DMA analysis—The DSC results shown in Fig. 2 confirm the immiscibility of TPU and PLA as can be verified from their completely separate glass transition slopes. As the TPU content increased, the glass transition temperature (T_g) of the two components did not change at all, while the slope of the TPU became steeper and the slope of the PLA became shallower. Fig. 2(a) shows that the PLA cold crystallization peak moved to a lower temperature and that the peak intensity became sharper in the PLA75% and PLA50% samples. These phenomena can be attributed to the added TPU, which acts as a crystallization nucleation agent by providing nucleation spots. Among the three blends, both the cold crystallization peak and the melting peak became smaller with an increase of TPU content. Fig. 2(b) shows the cooling scan data, from which it was noticed that the existence of PLA stimulated TPU crystallization, while the peak became stronger as the PLA content increased.

The energy depletion tan delta curves, whose peaks represent the glass transition temperatures of the materials, were determined from DMA testing (Fig. 3) and clearly show the immiscibility of TPU and PLA. The depletion peak for TPU was below zero and became weaker as PLA content increased. Similarly, the PLA depletion peak was approximately 80 °C and became smaller when the TPU content increased. All of the blends had two peaks at the same temperature which confirmed that PLA and TPU were completely immiscible. The sharp peak for the PLA indicated a rapid storage energy loss.

3.1.3. Phase morphology—SEM was used to further study the phase morphology of the PLA/TPU blends. The pure PLA and TPU fractured surface morphologies are shown in Fig. 4(a) and (b) for comparison. Fig. 4(c) through (e) show the phase morphology of the three blends. A large portion of the TPU spheres were uniformly inlaid in the PLA matrix and no obvious continuous TPU phase was observed in the PLA75% sample. The PLA50% sample had both PLA and TPU continuous phases, as well as some PLA spheres, as shown in Fig. 4(d). The PLA domain, however, formed islands in the TPU matrix (circled in the image) and there were fewer spheres than in the PLA75% sample. As shown in Fig. 4(e), PLA25% had tiny PLA spheres which were much smaller and less numerous than in PLA75% and were uniformly dispersed in the TPU matrix. In brief, clear phase separation was observed in all three PLA/TPU blends which further proved that PLA was completely immiscible with TPU.

3.2. Scaffold morphology

The microstructures of the microcellular injection molded samples are shown in Fig. 5. The morphology of pure PLA and TPU were significantly different and the pore structure varied between blends. It was found that the pore size of TPU was much larger than that of PLA and that more pores featured small holes that connected with other pores. The PLA75% sample (Fig. 5(c_1)) had a similar structure to pure PLA, while the morphology of the PLA25% (Fig. 5(e_1)) sample was close to that of pure TPU. PLA50% (Fig. 5(d_1)) had both large hollow voids and small pores. It is likely that the difference of scaffold microstructure could be attributed to the variety of phase morphologies. The PLA and TPU phase interface provided heterogeneous nucleation points during foaming [46]. The enlarged images show the phase morphology of the pore surface and pore wall. Pure materials (Fig. 5(a_2) and (b_2))

had relatively smooth surfaces, while the surfaces of the other three blends were rough. Large PLA spheres were found in the PLA75% scaffold, forming a rough pore wall and small hollow voids on the pore surface. One can clearly see the two phase morphologies in the PLA50% scaffold in both the pore wall and the pore surface from Fig. 5(d_2). The PLA25% scaffold (Fig. 5(e_2)) had tiny PLA spheres dispersed uniformly on the pore surface, thus forming a rough surface.

Statistical data pertaining to the porosity, average pore diameter, and pore density are shown in Fig. 6. It was found that the porosity showed a similar trend to the pore diameter and was inversely related to pore density. This was likely because larger pores were formed by merging smaller pores and expanding pore walls during foaming, inducing a reduction of pore density and an overall increase in porosity. As can be seen from Fig. 5, PLA75% and PLA25% had a similar porosity and pore diameter as compared to pure PLA and TPU, respectively. PLA 50%, however, had a lower pore diameter and porosity than the others. This might have been because the island phase of PLA in the TPU matrix prevented pore growth and led to both large and small pores in the sample, as shown in Fig. 5(d_1). Overall, microcellular injection molding fabricated scaffolds had average porosities ranging from 49% to 79%, pore diameters from 115 to 252 μm, and pore densities from 1.4×10^5 to $3.9 \times 10^5/cm^3$.

3.3. Mechanical and rheological properties

The tensile and compressive test results of solid and microcellular injection molded samples are shown in Fig. 7, and the tensile and compressive modulus results are shown in Fig. 8. Pure PLA had a high tensile modulus as well as a high compressive modulus, but it exhibited an extremely low elongation-at-break due to its brittle nature. Tensile and compressive yield stress decreased with the addition of TPU. Solid TPU samples and blend samples did not break during the tensile tests even when the strain reached 600%, as shown in Fig. 7(a). Fig. 7(b) shows that the strain-at-break increased with increasing TPU content for the microcellular injection molded samples and that the samples lost yield behavior when the TPU content increased to 75%. The compression tests showed similar results, as shown in Fig. 7(c) and (d). The compressive stress for microcellular injection molded samples was significantly lower than that of solid samples. According to Fig. 8, both the tensile and compressive moduli decreased as the TPU content increased. The tensile modulus of the microcellular injection molded samples was lower than that of the solid samples and ranged from 7 to 1,007 MPa, which can fulfill the requirement of tissues like cancellous bone, cartilage, ligament and tendon. The compressive modulus for microcellular injection molded samples ranged from 11 to 200 MPa, which meets the compressive modulus requirement of cancellous bone and cortical bone as introduced previously. Thus, the PLA/TPU scaffolds mass produced by microcellular injection molding have great potential in meeting the mechanical property requirements for human tissues.

In addition, polymer processing and autoclaving may cause polymer degradation which would further lead to a reduction of mechanical properties. Considering this, GPC tests were performed on raw TPU pellets, microcellular injection molded TPU scaffolds, and TPU scaffolds subjected to autoclave sterilization. It was found that the M_w of TPU decreased

gradually from 108.5 kDa (raw pellets), to 77.5 kDa (molded scaffold), and then to 75.7 kDa (autoclaved scaffold). The M_w results for PLA went from 91.8 kDa (raw pellets), to 85.9 kDa (molded scaffold), and then to 55.1 kDa (autoclaved scaffold). Interestingly, it was found that for TPU the most significant degradation happened during scaffold processing, whereas the autoclave process caused more degradation than scaffold processing for PLA. Therefore, autoclave sterilization may not be suitable for PLA (γ-radiation may be more appropriate as an alternative method), but it is still feasible for TPU.

PLA had a higher storage modulus than TPU according to thermal dynamic tests, as shown in Fig. 9. The storage modulus curves of the three blends were located between PLA and TPU for both solid and microcellular injection molded samples as expected. Interestingly, it was noticed that both solid and microcellular injection molded PLA25% samples had a relatively high storage modulus at low temperature, which might be because of the reinforcement behavior of rigid PLA spheres dispersed in the TPU matrix as previously shown by the phase morphology images. However, as the temperature increased, the storage modulus dropped rapidly so that no improvement was observed in the tensile and compression tests that were performed at room temperature.

As shown in Fig. 10, the complex viscosity increased along with the amount of TPU because pure TPU had a higher viscosity than pure PLA. The reinforcement behavior of PLA25% was also observed in rheology tests at low angular frequency. Together with the storage modulus results, it is possible that the tiny PLA spheres in PLA25% were acting as rigid fillers which had a slow response to frequency at low temperatures and low frequency at high temperatures. The PLA 50% samples had a continuous PLA phase and the PLA75% samples had large PLA spheres and a small TPU domain such that no reinforcement behavior was observed in them.

3.4. Cell viability and proliferation

The 3T3 fibroblast cell viability and morphology Day 3 and Day 10 results are shown in Figs. 11 and 12. From the images it is clear that fibroblasts attached and spread all over the scaffolds. The fluorescence images show large quantities of live cells. By comparing Fig. 11(a) through (c), it was found that the dispersion of dead cells was uniform for PLA and PLA50% scaffolds, while most dead cells were located in the center solid area of the TPU scaffold at Day 3.

The fibroblast cell morphologies of the three scaffolds are shown in Fig. 11(d) through (i). At Day 3, most cells attached to the solid area, with some already covering the pores on the PLA and PLA50% scaffolds. Fewer cells were observed on the TPU scaffold and fewer pores had been covered than in the other two scaffolds as well. Nevertheless, cells can be seen migrating inside of the pores in Fig. 11(i). The Day 10 fluorescence images (Fig. 12(a) through (c)) show that very few dead cells were present on all three scaffolds. The media was relatively clear, suggesting that not many dead cells were washed away during periodic culture media replacement. It was observed that live cells continued to proliferate on the scaffolds which indicated that the scaffolds provided a suitable ECM for cells to grow. The SEM pictures (Fig. 12(d) through (i)) show the morphology of cells at low and high magnifications. From these images it was noticed that a lot of cells were growing on, and

almost covering, the entire scaffolds. Although PLA and PLA50% scaffolds had denser cell populations than TPU scaffolds, the fibroblast cells stretched and spread very well on all of the scaffolds. The MTS assay statistical data of Day 3 and Day 10 cell counts is shown in Fig. 13, and showed that cell populations increased from Day 3 to Day 10 dramatically on all scaffolds. Thus it was shown that the scaffolds fabricated by microcellular injection molding could support cell growth very well. Moreover, the PLA scaffold had a higher average number of cells than the PLA50% scaffold, which was higher than the TPU scaffold. However, from the Student's *t*-test analysis, it was found that the number of cells on the PLA scaffold at Day 3 was the only scaffold that was significantly better than the other two scaffolds at the same time point using a 95% ($p < 0.05$) confidence level. Thus, all three kinds of scaffolds are suitable for fibroblast cell culture and one could assume that the other two scaffolds, PLA25% and PLA50%, would be appropriate for cell culture as well. Therefore, scaffolds with a variety of properties that are potentially suitable for different tissue applications were successfully fabricated via microcellular injection molding in this study.

4. Conclusion

TPU and PLA were melt blended with a twin-screw extruder and microcellular injection molded to mass produce tissue engineering scaffolds with different ratios and resulting mechanical properties and phase morphologies. The properties of pure materials and blends were investigated via multiple characterization methods. It was found that the PLA and TPU used in this study were completely immiscible and that the PLA dispersed as small spheres at 25%, or large spheres at 75%, in the TPU matrix, and formed into both spheres and islands at 50%. Mechanical tests confirmed the large tensile and compressive range of the scaffolds fabricated by microcellular injection molding which may be potentially used in multiple tissue applications. The elongation-at-break improved dramatically as the TPU content increased in the blends. The scaffolds fabricated in this study had porosities ranging from 49% to 79%, pore diameters from 115 to 252 μm, and pore densities from 1.4×10^5 to $3.9 \times 10^5/cm^3$. Furthermore, the pores were relatively larger for the scaffolds with a higher TPU content. Dynamic mechanical tests and rheology tests found that the tiny dispersed PLA spheres in the TPU matrix at 25% reinforced the blends at low temperatures or low frequencies. 3T3 fibroblast cell culture experiments demonstrated the biocompatibility of the scaffolds and that scaffolds with more PLA content had slightly higher cell viabilities, although not at a statistically significant level ($p < 0.05$). In light of the biocompatibility, tunable mechanical properties, and porous microstructure, the scaffolds fabricated via microcellular injection molding have the potential to be used for multiple tissue types in a variety of medical and tissue engineering applications.

Acknowledgements

The authors would like to acknowledge the support of the Wisconsin Institute for Discovery (WID), the China Scholarship Council, the financial support of the National Nature Science Foundation of China (No. 51073061, No. 21174044), the Fundamental Research Funds for the Central Universities (No. 2011ZZ0011), the 973 Program (2012CB025902), the National Institutes of Health (Grant Number K18HL105504 from the National Heart, Lung, and Blood Institute), and the Graduate School of the University of Wisconsin-Madison. The content is solely the responsibility of the authors and does not necessarily represent the official views of the aforementioned organizations.

References

[1]. Langer R, Vacanti JP. Science. 1993; 260:920–926. [PubMed: 8493529]

[2]. Weinand C, Pomerantseva I, Neville CM, Gupta R, Weinberg E, Madisch I, Shapiro F, Abukawa H, Troulis MJ, Vacanti JP. Bone. 2006; 38:555–563. [PubMed: 16376162]

[3]. Wang XW, Lin P, Yao QH, Chen CY. World J. Surg. 2007; 31:682–689. [PubMed: 17345123]

[4]. Zhang YZ, Venugopal J, Huang ZM, Lim CT, Ramakrishna S. Biomacromolecules. 2005; 6:2583–2589. [PubMed: 16153095]

[5]. Yang SF, Leong KF, Du ZH, Chua CK. Tissue Eng. 2001; 7:679–689. [PubMed: 11749726]

[6]. Kramschuster A, Turng LS. J. Biomed. Mater. Res. B. 2010; 92B:366–376.

[7]. Baji A, Wong SC, Srivatsan TS, Njus GO, Mathur G. Mater. Manuf. Process. 2006; 21:211–218.

[8]. Oh SH, Kang SG, Kim ES, Cho SH, Lee JH. Biomaterials. 2003; 24:4011–4021. [PubMed: 12834596]

[9]. Shor L, Yildirim ED, Guceri S, Sun W. Biol. Med. Phys. Biomed. Eng. 2010:91–110.

[10]. Yeo A, Wong WJ, Teoh SH. J. Biomed. Mater. Res. A. 2010; 93A:1358–1367. [PubMed: 19911382]

[11]. Ajami-Henriquez D, Rodriguez M, Sabino M, Castillo RV, Muller AJ, Boschetti-de-Fierro A, Abetz C, Abetz V, Dubois P. J. Biomed. Mater. Res. A. 2008; 87A:405–417. [PubMed: 18186046]

[12]. Geiger M, Li RH, Friess W. Adv. Drug Deliv. Rev. 2003; 55:1613–1629. [PubMed: 14623404]

[13]. Li C, Wang LL, Yang Z, Kim G, Chen HF, Ge ZG. J. Biomater. Sci. Polym. Ed. 2012; 23:405–424. [PubMed: 21310105]

[14]. Montjovent MO, Mark S, Mathieu L, Scaletta C, Scherberich A, Delabarde C, Zambelli PY, Bourban PE, Applegate LA, Pioletti DP. Bone. 2008; 42:554–564. [PubMed: 18178142]

[15]. Mondrinos MJ, Dembzynski R, Lu L, Byrapogu VKC, Wootton DM, Lelkes PI, Zhou J. Biomaterials. 2006; 27:4399–4408. [PubMed: 16678255]

[16]. Lian C, Wei L, Yilin C. J. Tissue Eng. Regen. Med. 2012; 6:214–214. [PubMed: 21442765]

[17]. Buschmann J, Harter L, Gao SP, Hemmi S, Welti M, Hild N, Schneider OD, Stark WJ, Lindenblatt N, Werner CML, Wanner GA, Calcagni M. Injury. 2012; 43:1689–1697. [PubMed: 22769980]

[18]. Hofmann A, Ritz U, Verrier S, Eglin D, Alini M, Fuchs S, Kirkpatrick CJ, Rommens PM. Biomaterials. 2008; 29:4217–4226. [PubMed: 18692894]

[19]. Son JS, Teja G, Appleford M, Ong JL, Park K, Han DK, Oh S. Tissue Eng. Regen. Med. 2009; 6:1241–1251.

[20]. Wang SD, Zhang YZ, Yin GB, Wang HW, Dong ZH. J. Appl. Polym. Sci. 2009; 113:2675–2682.

[21]. Lohmann CH, Schwartz Z, Niederauer GG, Carnes DL, Dean DD, Boyan BB. Biomaterials. 2000; 21:49–61. [PubMed: 10619678]

[22]. Haroosh HJ, Chaudhary DS, Dong Y. J. Appl. Polym. Sci. 2012; 124:3930–3939.

[23]. Liu X, Huang CB, Feng YJ, Liang J, Fan YJ, Gu ZW, Zhang XD. J. Biomater. Sci. Polym. Ed. 2010; 21:963–977. [PubMed: 20482996]

[24]. Niu XF, Li XM, Liu HF, Zhou G, Feng QL, Cui FZ, Fan YB. J. Biomater. Sci. Polym. Ed. 2012; 23:391–404. [PubMed: 21255484]

[25]. Liu H, Wang SD, Qi N. J. Appl. Polym. Sci. 2012; 125:E468–E476.

[26]. Diao HX, Si YF, Zhu AP, Ji LJ, Shi HC. Mater. Sci. Eng. C. 2012; 32:1796–1801.

[27]. Kong YX, Yuan J, Qiu J. Physica B. 2012; 407:2451–2457.

[28]. Guelcher SA. Tissue Eng. Part B Rev. 2008; 14:3–17. [PubMed: 18454631]

[29]. Gorna K, Gogolewski S. Polym. Degrad. Stab. 2002; 75:113–122.

[30]. Hentschel T, Munstedt H. Infection. 1999; 27:S43–S45. [PubMed: 10379443]

[31]. Santerre JP, Woodhouse K, Laroche G, Labow RS. Biomaterials. 2005; 26:7457–7470. [PubMed: 16024077]

[32]. Segal E, Tchoudakov R, Narkis M, Siegmann A. Polym. Eng. Sci. 2002; 42:2430–2439.

[33]. Huang C, Chen R, Ke QF, Morsi Y, Zhang KH, Mo XM. Colloids Surf. B. 2011; 82:307–315.
[34]. Burke A, Hasirci N. Adv. Exp. Med. Biol. 2004; 553:83–101. [PubMed: 15503449]
[35]. Ping P, Wang WS, Zhang PB, Chen XS, Jing XB. Chem. J. Chin. Univ. 2007; 28:371–375.
[36]. Hong H, Wei J, Yuan YA, Chen FP, Wang J, Qu X, Liu CS. J. Appl. Polym. Sci. 2011; 121:855–861.
[37]. Mikos AG, Thorsen AJ, Czerwonka LA, Bao Y, Langer R, Winslow DN, Vacanti JP. Polymer. 1994; 35:1068–1077.
[38]. Nakamatsu J, Torres FG, Troncoso OP, Yuan ML, Boccaccini AR. Biomacromolecules. 2006; 7:3345–3355. [PubMed: 17154462]
[39]. Wang L, Shi J, Liu L, Secret E, Chen Y. Microelectron. Eng. 2011; 88:1718–1721.
[40]. Park SA, Kim HJ, Lee SH, Lee JH, Kim HK, Yoon TR, Kim W. Polym. Eng. Sci. 2011; 51:1883–1890.
[41]. Corre YM, Maazouz A, Duchet J, Reignier J, Supercrit J. Fluids. 2011; 58:177–188.
[42]. Gerhardt LJ, Manke CW, Gulari E. J. Polym. Sci. Polym. Phys. 1997; 35:523–534.
[43]. Wu HB, Haugen HJ, Wintermantel E. J. Cell. Plast. 2012; 48:141–159.
[44]. Dong ZH, Li YB, Zou Q. Appl. Surf. Sci. 2009; 255:6087–6091.
[45]. Yang XZ, Wang YC, Tang LY, Xia H, Wang J. J. Polym. Sci. A Polym. Chem. 2008; 46:6425–6434.
[46]. Leung SN, Park CB, Li H. Plast. Rubber Compos. 2006; 35:93–100.

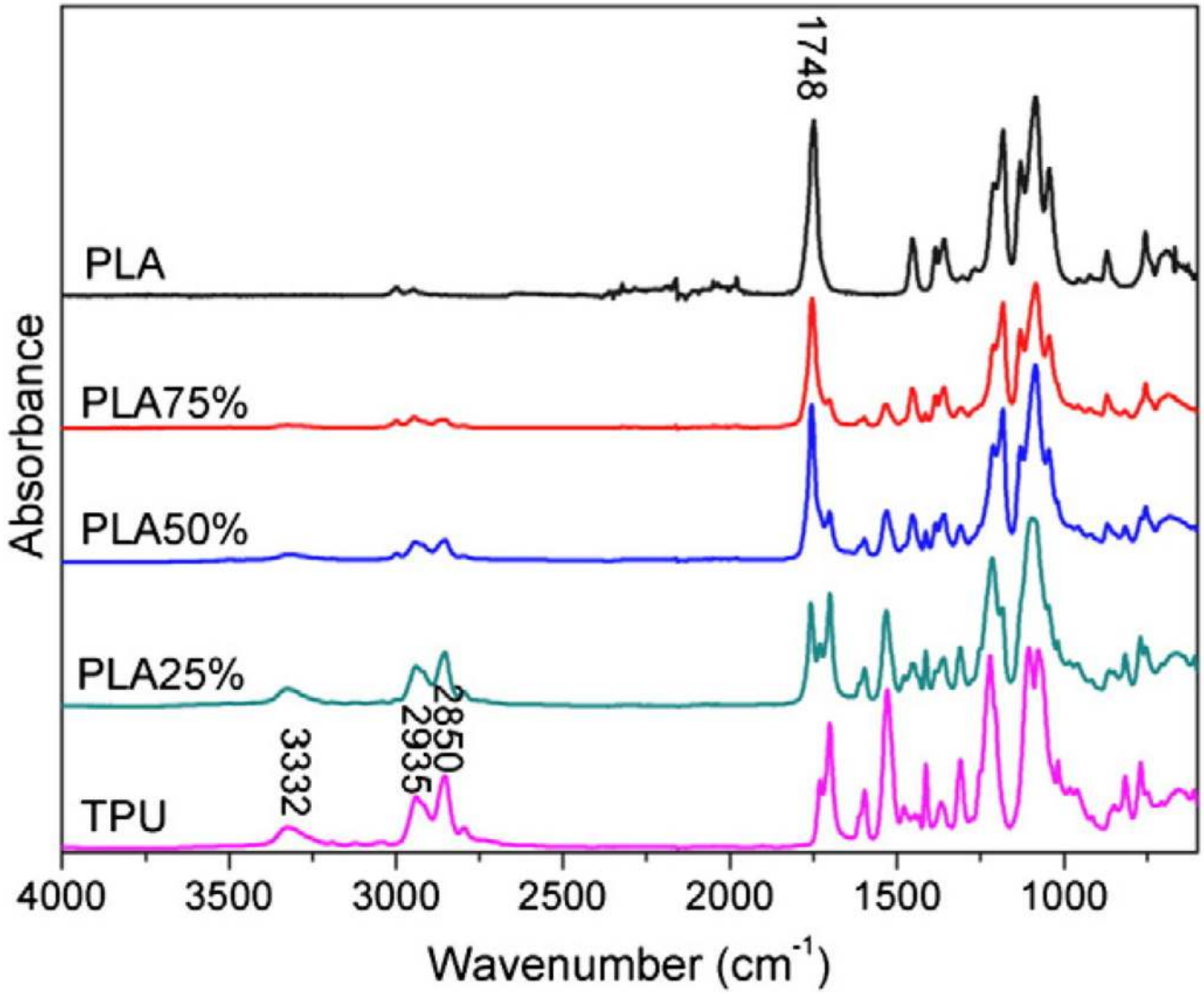

Fig. 1.
FTIR results of PLA, PLA75%, PLA50%, PLA25%, and TPU samples.

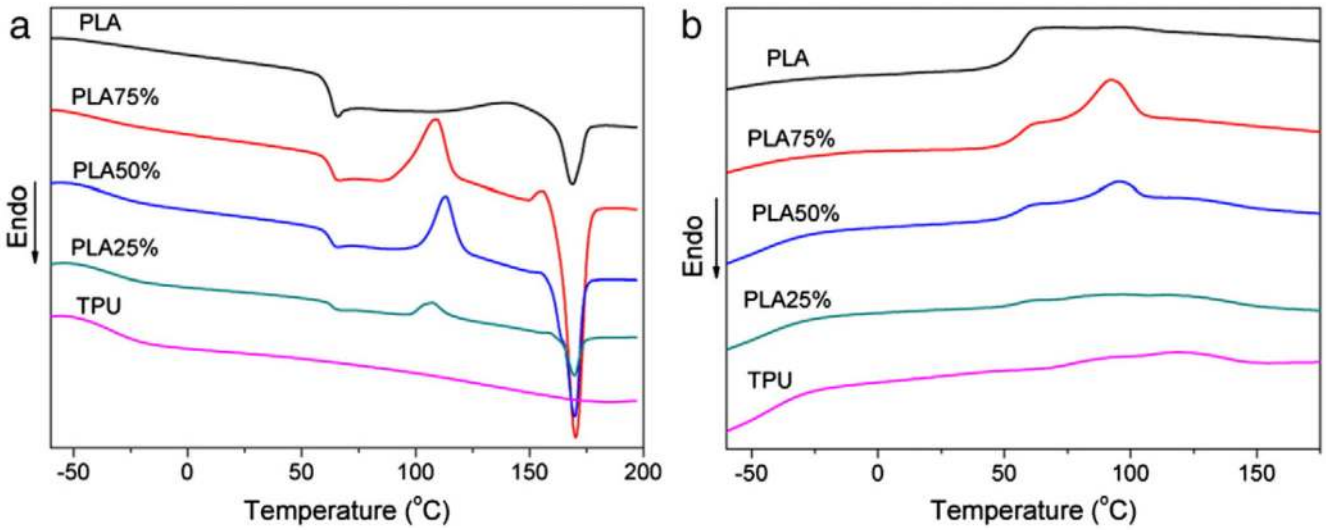

Fig. 2.

DSC (a) second heating and (b) cooling results of PLA, PLA75%, PLA50%, PLA25% and TPU samples.

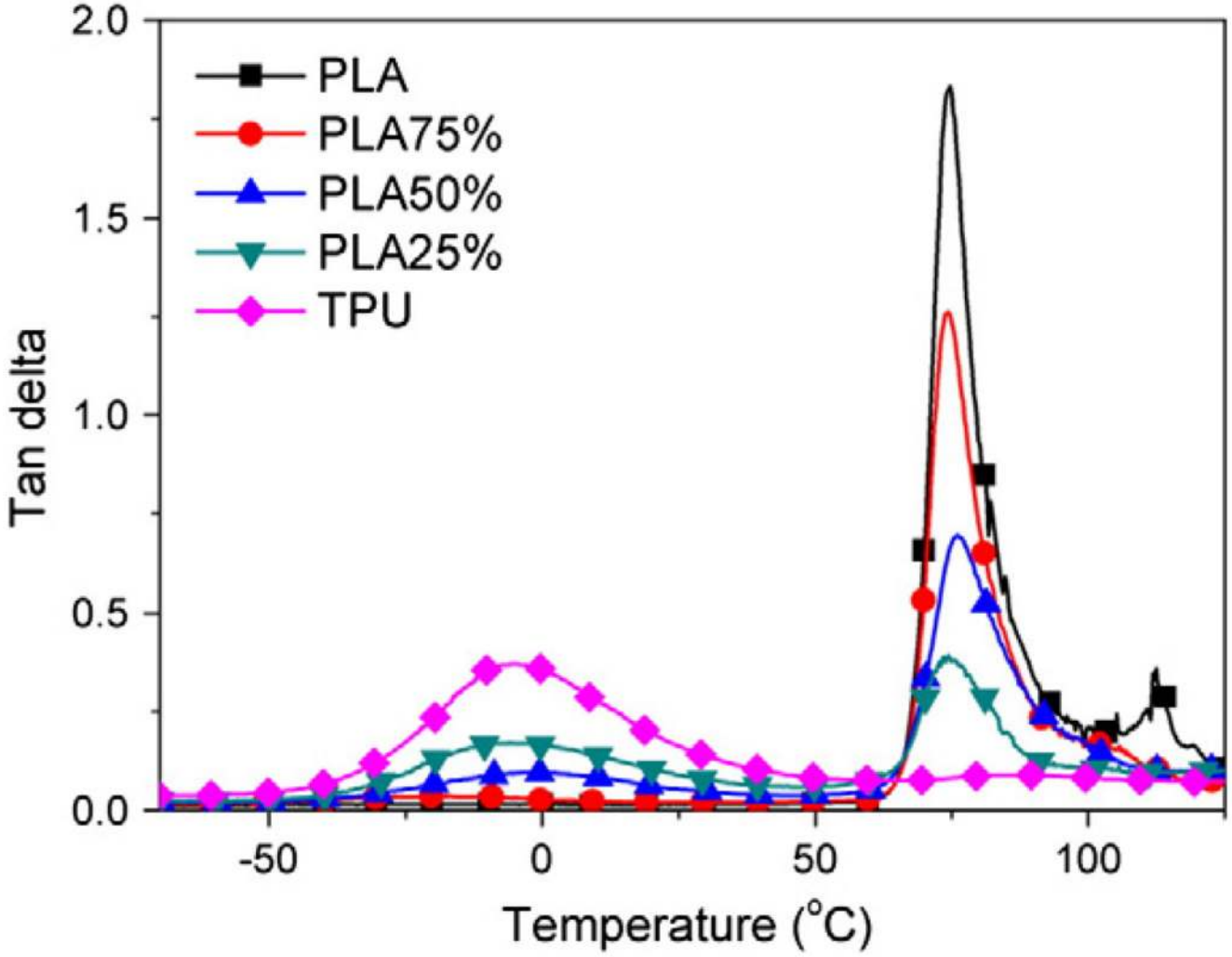

Fig. 3.
DMA tan delta results PLA, PLA75%, PLA50%, PLA25%, and TPU samples.

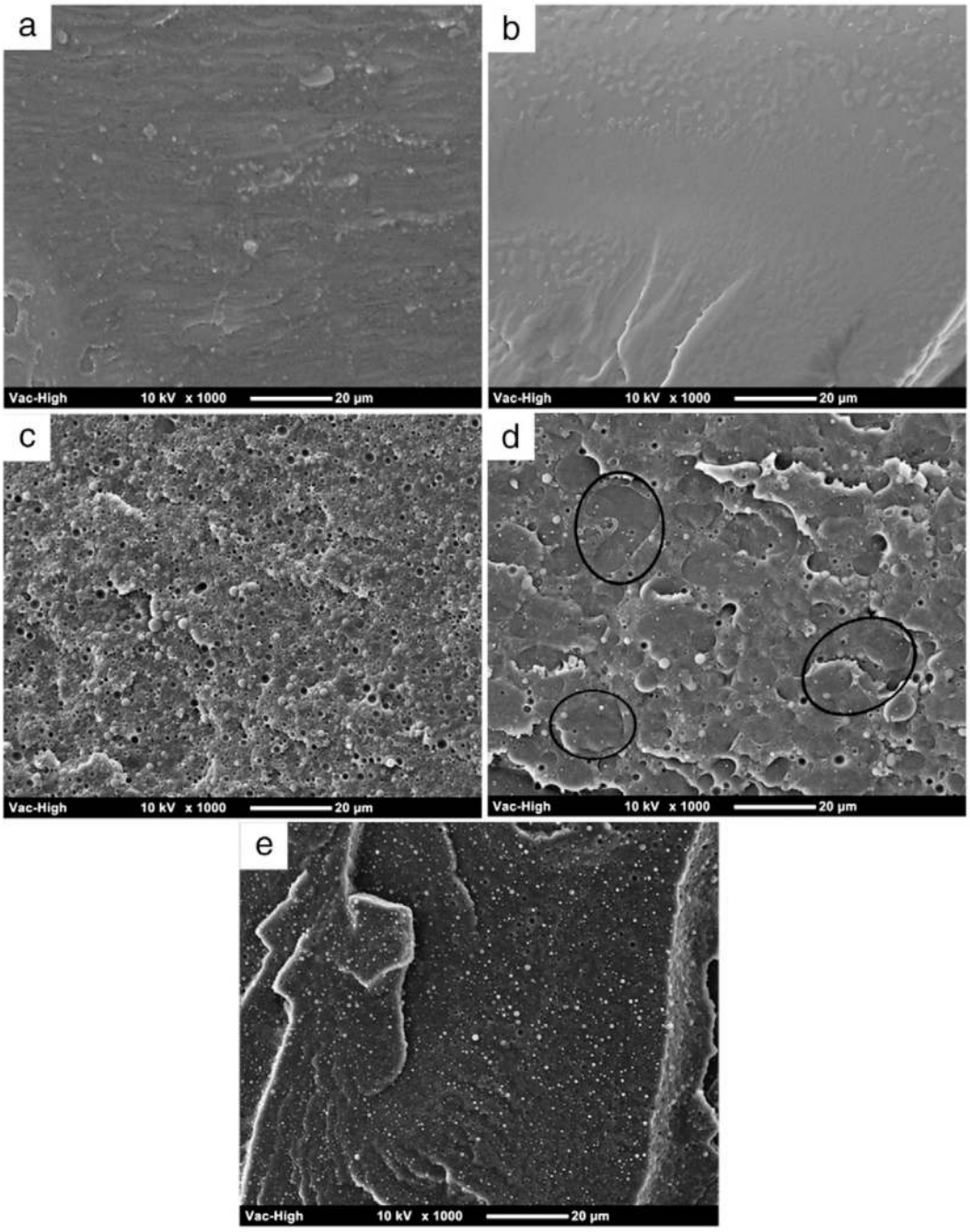

Fig. 4.
SEM phase morphology of (a) PLA, (b) TPU, (c) PLA75%, (d) PLA50%, and (e) PLA25% solid samples.

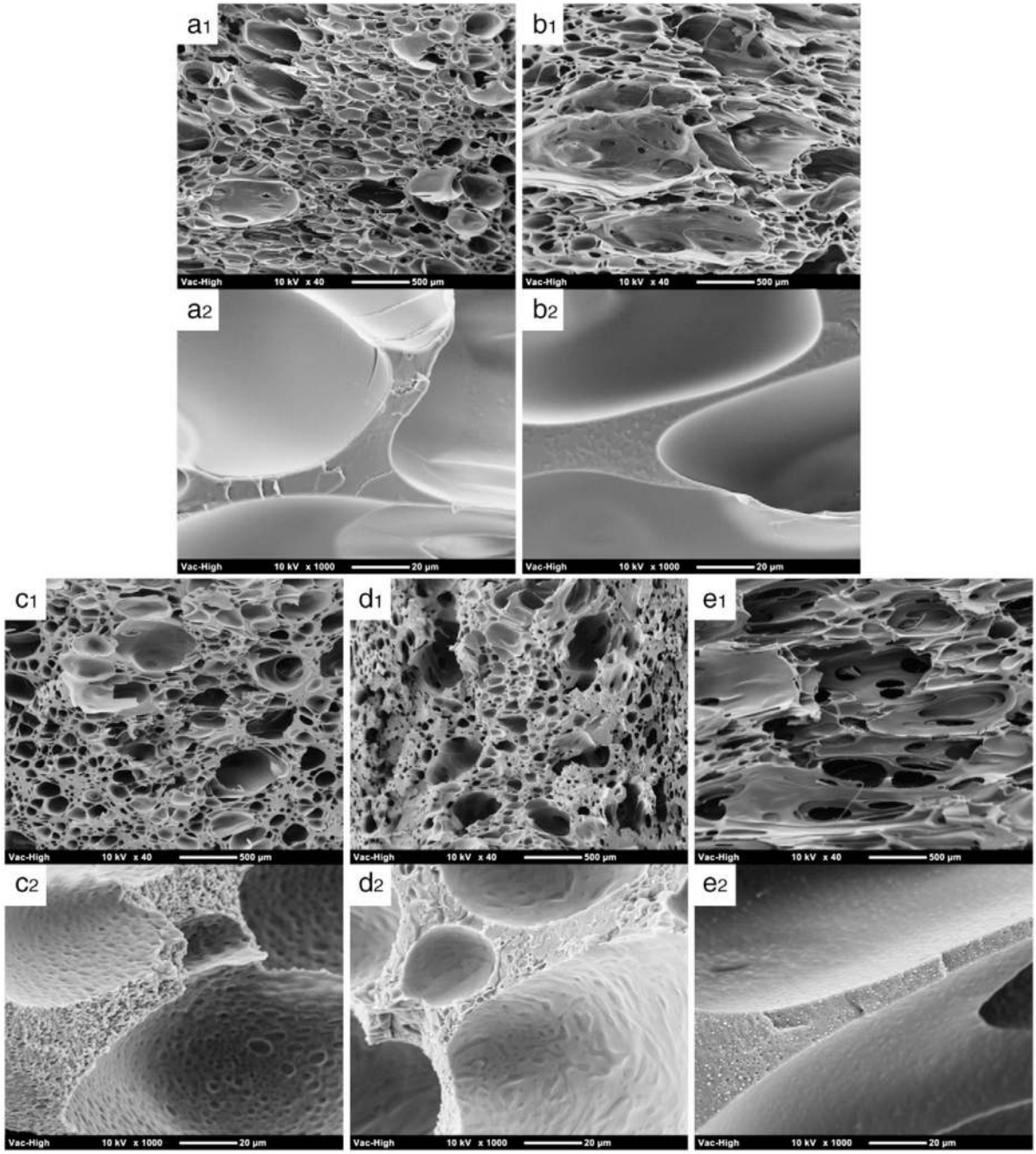

Fig. 5.

SEM images of microcellular injection molded scaffolds: (a) PLA, (b) TPU, (c) PLA75%, (d) PLA50%, and (e) PLA 25%. Subscript 2 images are enlarged images of subscript 1 images. Scale bars are 500 µm and 20 µm, respectively.

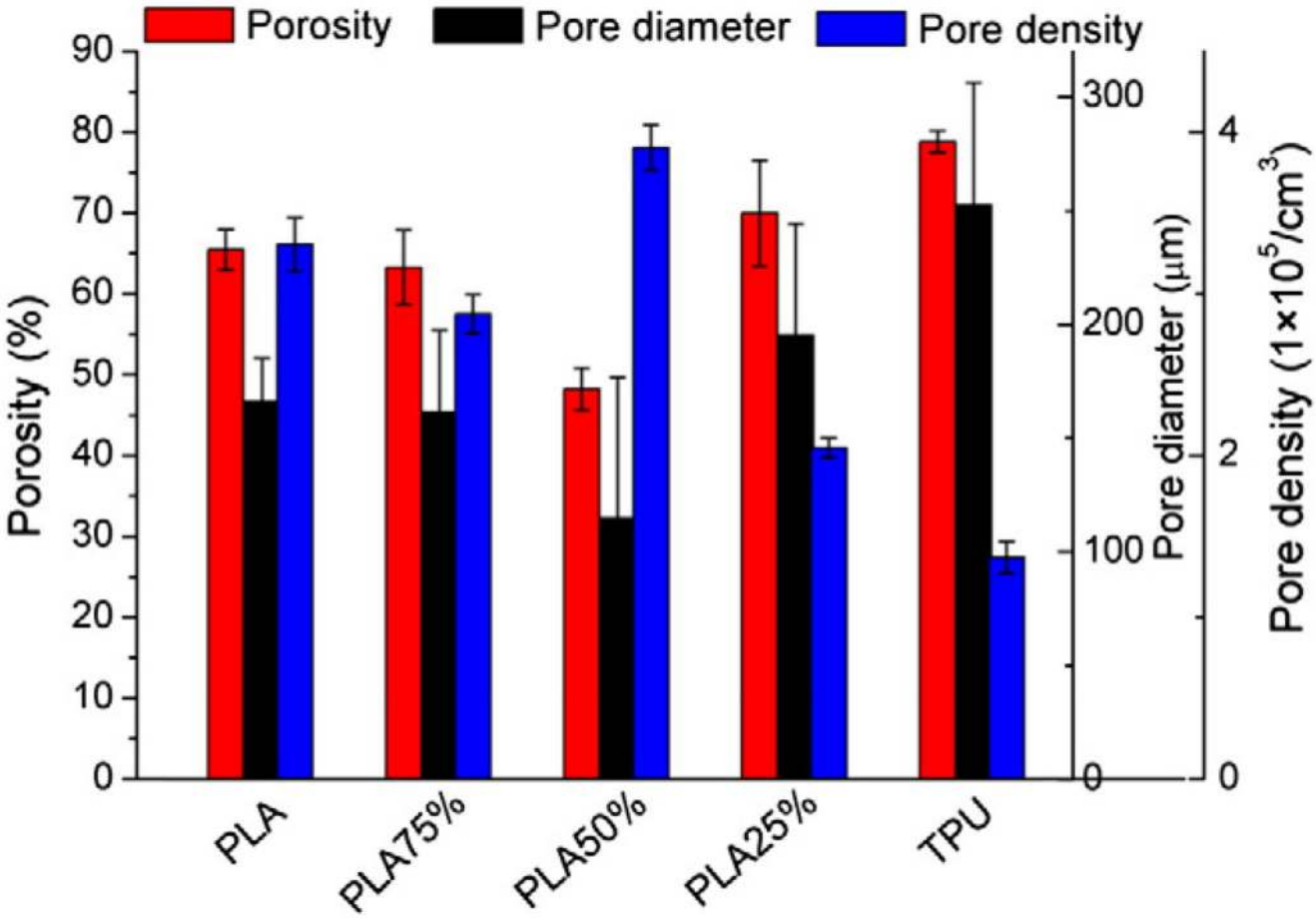

Fig. 6.

Porosity, pore diameter, and pore density statistical results of PLA, PLA75%, PLA50%, PLA25%, and TPU scaffolds.

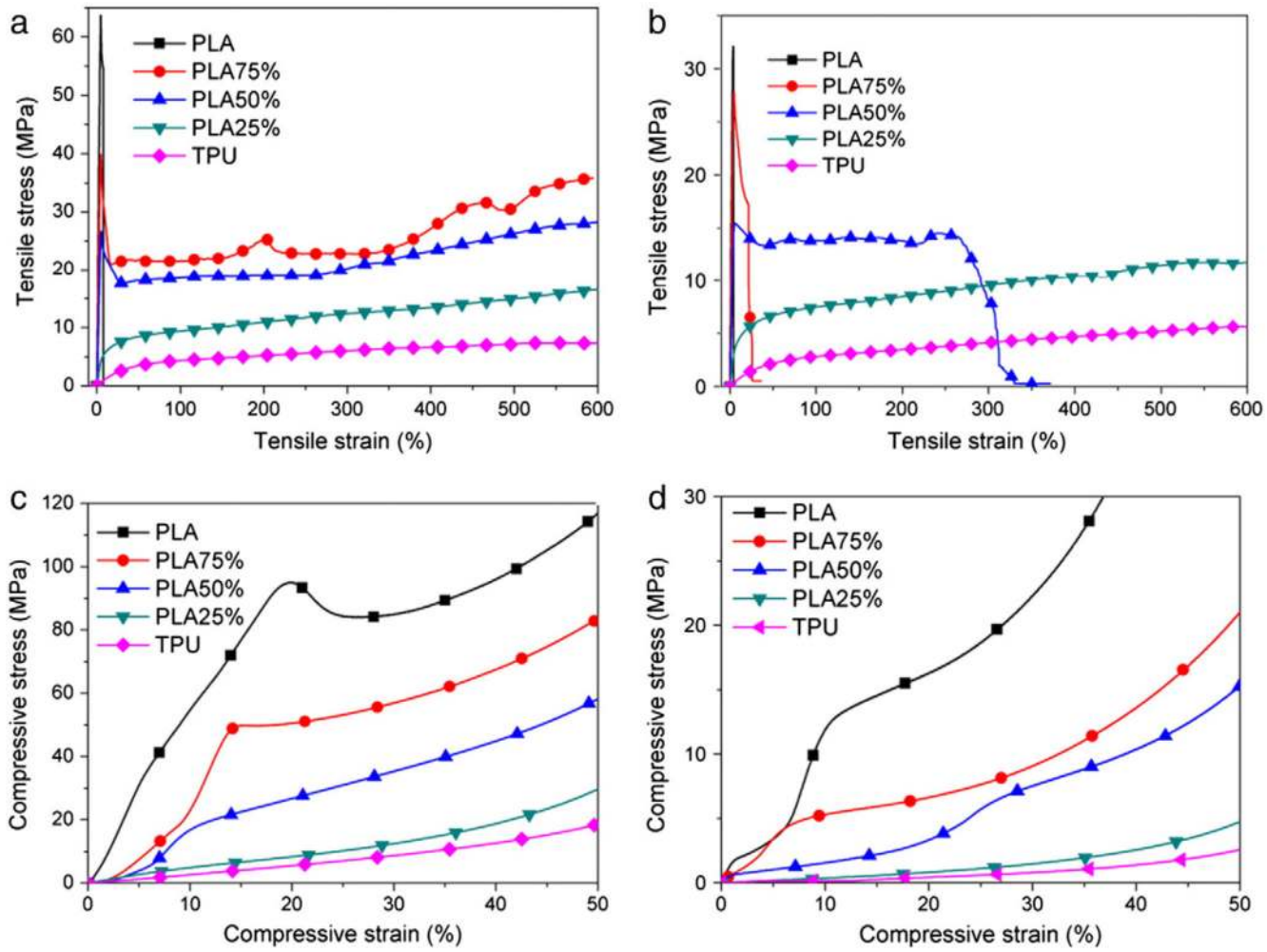

Fig. 7.

Mechanical property tests: (a) tensile test of solid samples, (b) tensile test of microcellular injection molded scaffolds, (c) compressive test of solid samples, and (d) compressive test of microcellular injection molded scaffolds.

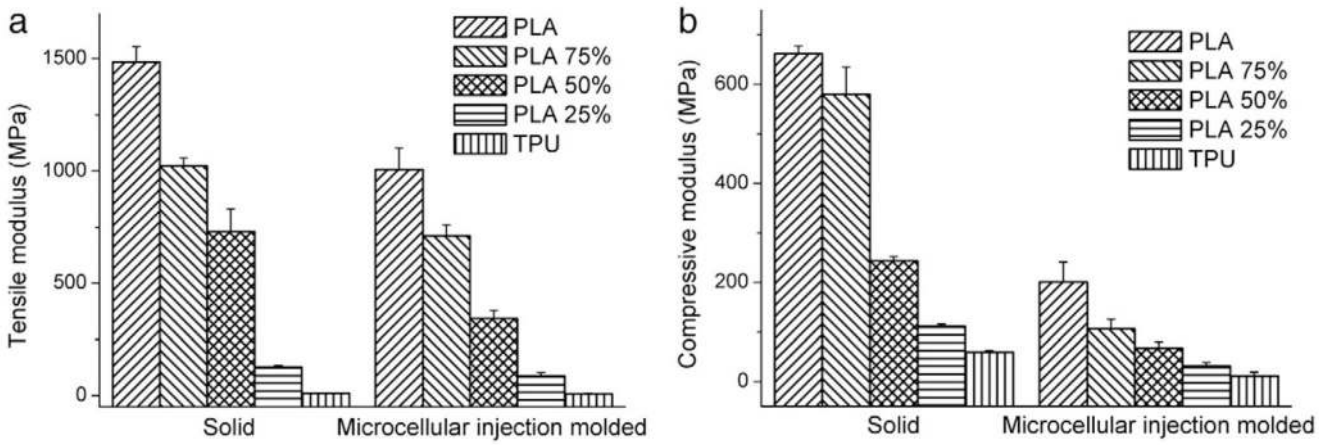

Fig. 8.

Statistical histogram of (a) tensile modulus and (b) compressive modulus for both solid samples and microcellular injection molded scaffolds.

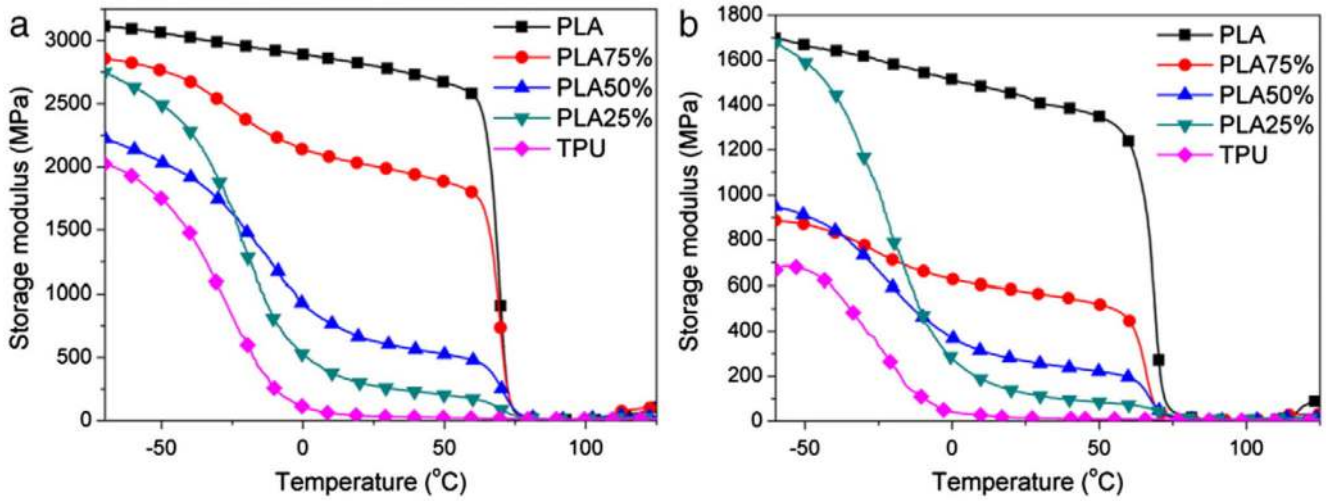

Fig. 9.

DMA storage modulus of PLA, PLA75%, PLA50%, PLA25%, and TPU: (a) solid samples and (b) microcellular injection molded scaffolds.

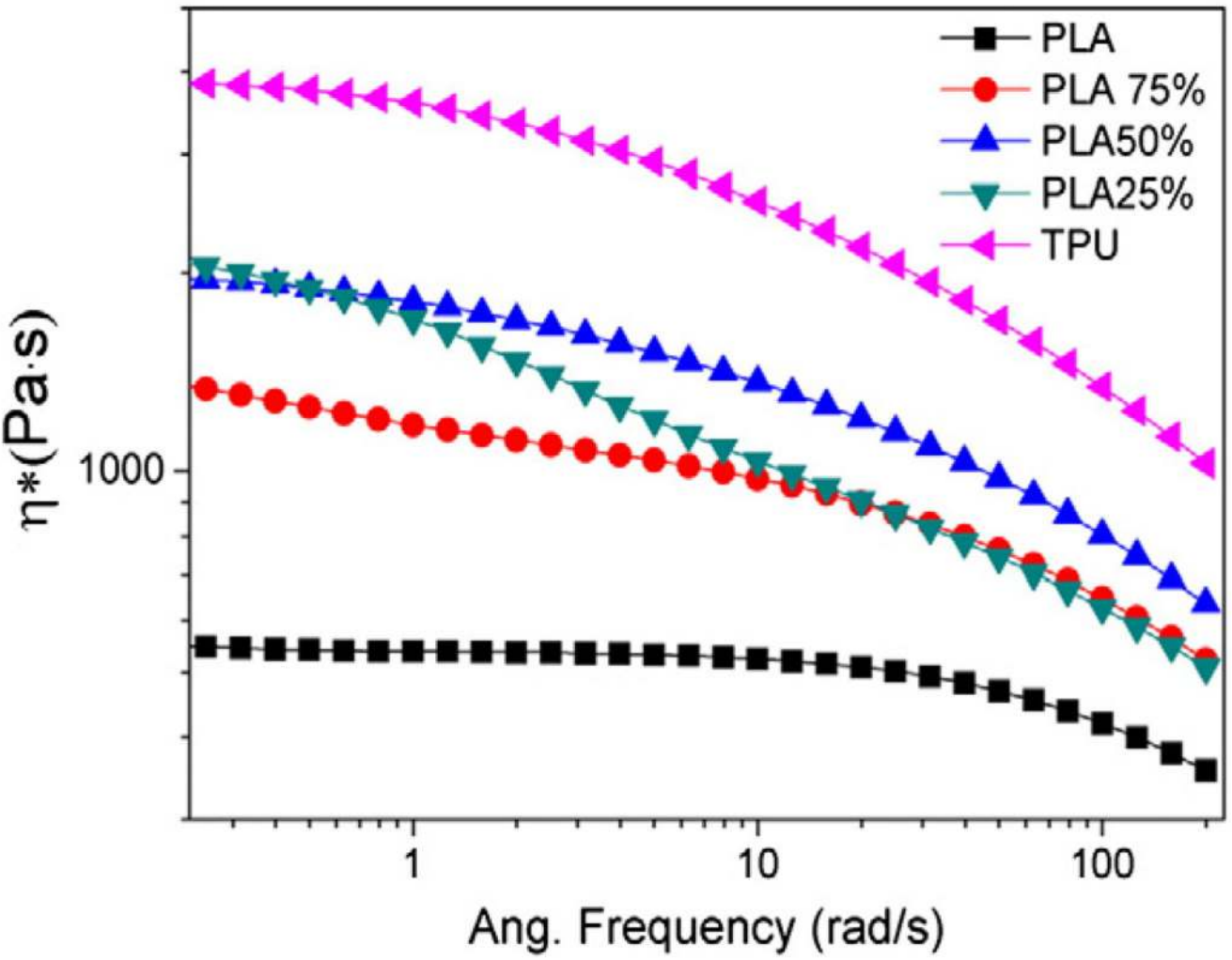

Fig. 10.
Rheology tests of PLA, PLA75%, PLA50%, PLA25%, and TPU blends (compounded pellets).

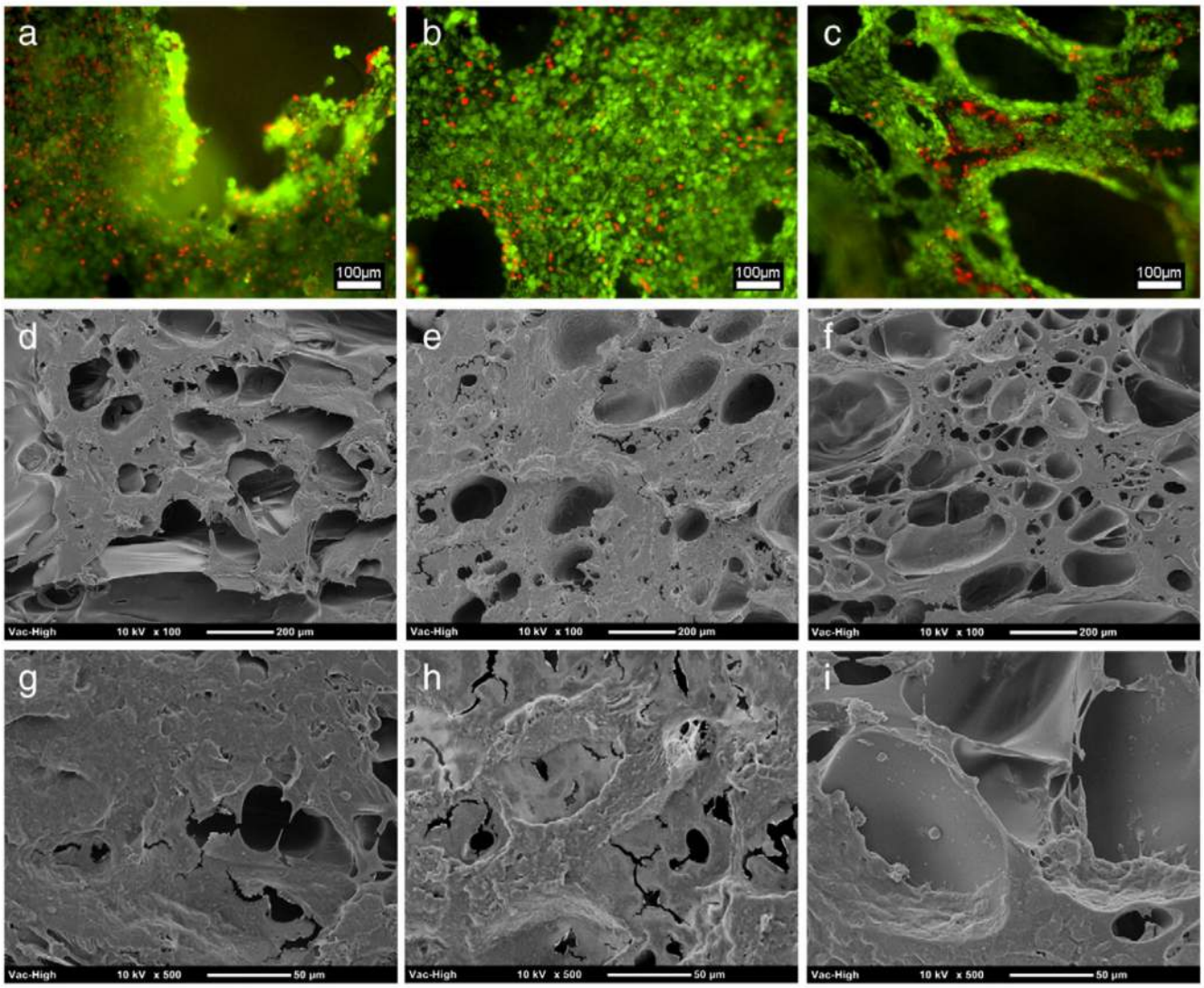

Fig. 11.

Day 3 fibroblast cell culture results of microcellular injection molded PLA (a, d, g), PLA50% (b, e, h), and TPU (c, f, i) scaffolds: (a–c) are fluorescence microscope pictures (scale bar = 100 μm) where green indicates living cells and red indicates dead cells, (d–f) are low magnification SEM images (scale bar = 200 μm), and (g–i) are high magnification SEM images (scale bar = 50 μm).

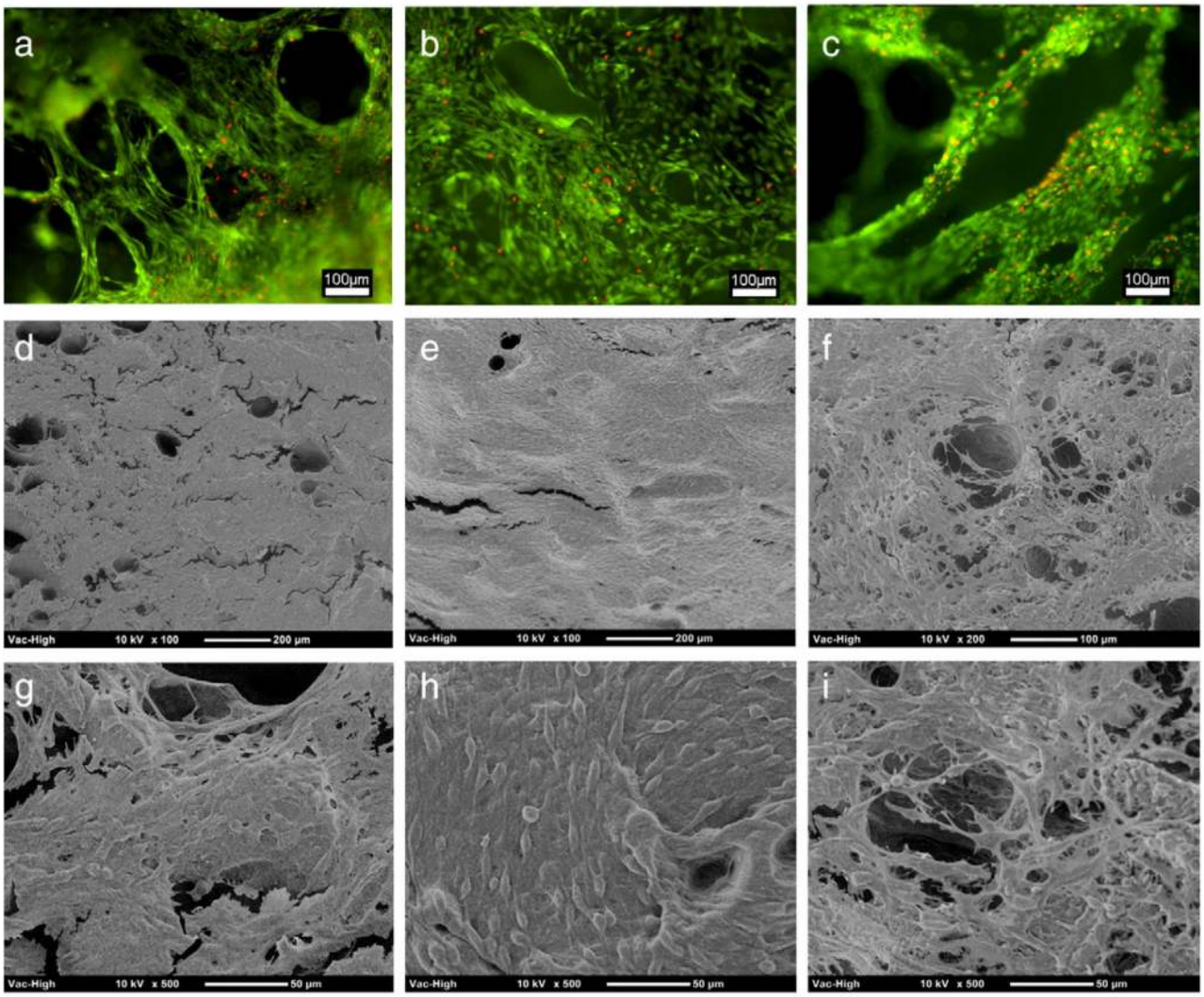

Fig. 12.

Day 10 fibroblast cell culture results of microcellular injection molded PLA (a, d, g), PLA50% (b, e, h), and TPU (c, f, i) scaffolds: (a-c) are fluorescence microscope pictures (scale bar = 100 μm) where green indicates living cells and red indicates dead cells, (d-f) are low magnification SEM images (scale bar = 200 μm for d and e, 100 μm for f), and (g-i) are high magnification SEM images (scale bar = 50 μm).

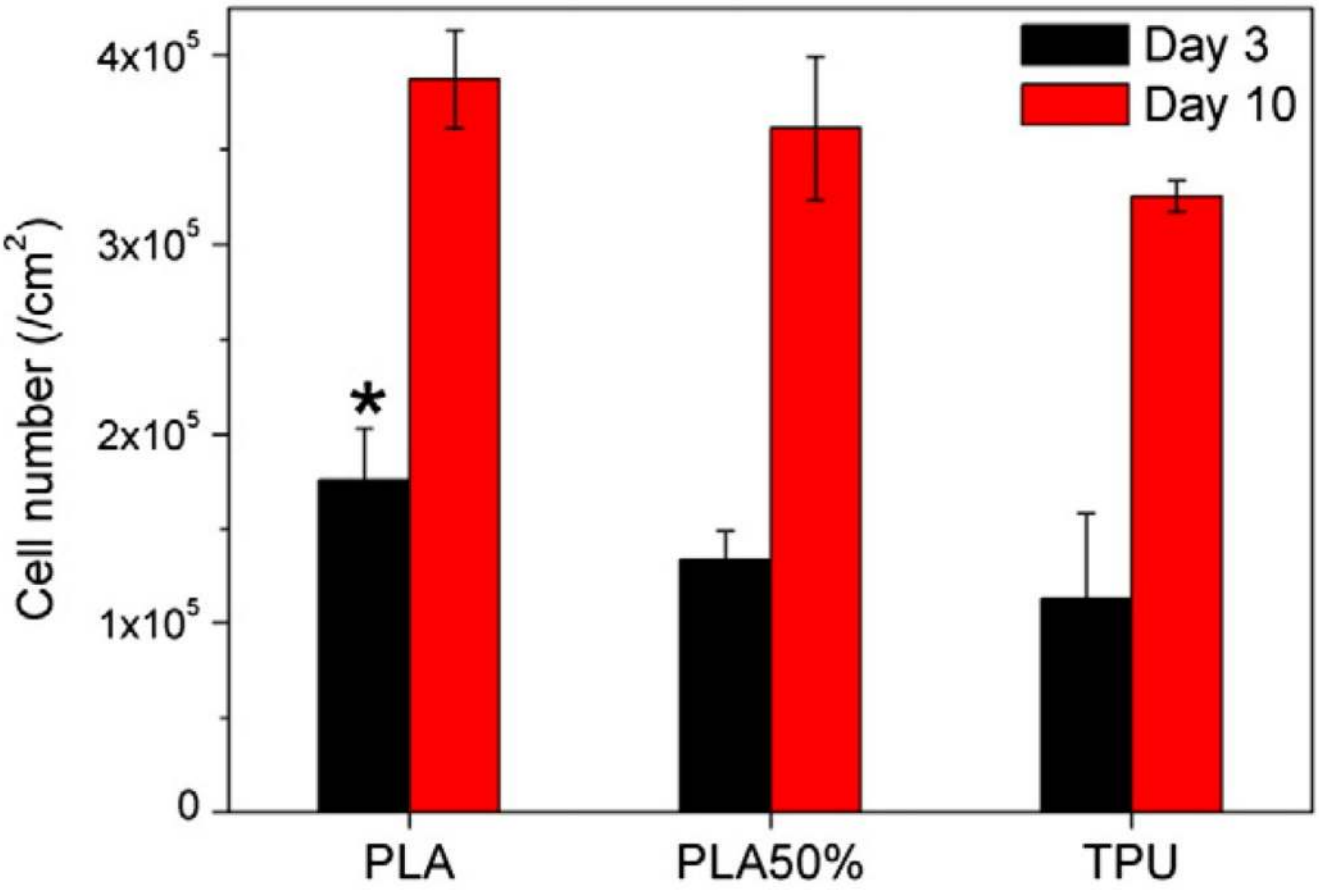

Fig. 13.

MTS assay cell count statistical results of microcellular injection molded PLA, PLA50%, and TPU scaffolds at Day 3 and Day 10 time points (significance level $p < 0.05$).

Table 1

Mechanical properties of several human tissues [5-7].

	Tensile strength (MPa)	Compressive strength (MPa)	Young's modulus (MPa)
Cancellous bone	8	4–12	50–100
Cortical bone	60–160	130–180	$3–30 \times 10^3$
Cartilage	3.7–10.5	n/a	0.7–15.3
Ligament	13–46	n/a	65–541
Tendon	24–112	n/a	143–2310

Table 2

Processing parameters.

Molding parameters	Value
Cooling time	60 s
Clamp tonnage	200 kN
Mold temperature	23 °C
CO_2 content	4 wt.%
Injection volume	70 vol.%
Injection speed	20 cm^3/s
Plasticizing temperature	190 °C
Back pressure	6 MPa